Macromolecules

Article

pubs.acs.org/Macromolecules

# Polymer/Polymer Blend Solar Cells Using Tetraazabenzodifluoranthene Diimide Conjugated Polymers as Electron Acceptors

Haiyan Li,[†] Ye-Jin Hwang,[†] Taeshik Earmme,[†] Rachel C. Huber,[‡] Brett A. E. Courtright,[†] Conor O'Brien,[†] Sarah H. Tolbert,[‡,§] and Samson A. Jenekhe*,[†]

[†]Department of Chemical Engineering and Department of Chemistry, University of Washington, Seattle, Washington 98195-1750, United States

[‡]Department of Chemistry and Biochemistry and the California NanoSystems Institute, University of California, Los Angeles, Los Angeles, California 90095-1569, United States

[§]Department of Materials Science and Engineering, University of California, Los Angeles, Los Angeles, California 90095, United States

Supporting Information

**ABSTRACT:** Two n-type semiconducting polymers with alternating arylene (thiophene or selenophene)−tetraazabenzodifluoranthene diimide (BFI) donor−acceptor architecture have been investigated as new electron acceptors in polymer/polymer blend solar cells. The new selenophene-linked polymer, PBFI-S, has a significantly smaller optical band gap (1.13 eV) than the thiophene-linked PBFI-T (1.38 eV); however, both polymers have similar HOMO/LUMO energy levels determined from cyclic voltammetry. Blends of PBFI-T with the thiazolothiazole−dithienylsilole donor polymer (PSEHTT) gave a 2.60% power conversion efficiency (PCE) with a 7.34 mA/cm$^2$ short-circuit current. In contrast, PBFI-S:PSEHTT blends had a 0.75% PCE with similarly reduced photocurrent and external quantum efficiency. Reduced free energy for charge transfer and reduced bulk electron mobility in PBFI-S:PSEHTT blends compared to PBFI-T:PSEHTT blends as well as significant differences in bulk film morphology are among the reasons for the large loss in efficiency in PBFI-S:PSEHTT blend solar cells.

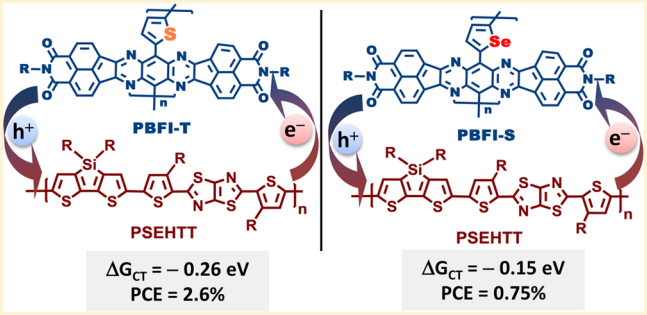


## INTRODUCTION

Advances in the design and synthesis of hole-conducting (p-type or donor) polymer semiconductors[1−3] in the past two decades have enabled major progress in developing increasingly more efficient polymer/fullerene bulk heterojunction (BHJ) solar cells.[4−13] Since the donor polymer is the main absorber in such fullerene acceptor-based organic photovoltaics (OPVs), the charge photogeneration process critically depends on efficiency of electron transfer from the photoexcited polymer to the fullerene derivative, such as [6,6]-phenyl-$C_{60}$-butyric acid methyl ester ($PC_{61}BM$) or [6,6]-phenyl-$C_{70}$-butyric acid methyl ester ($PC_{71}BM$). It is expected that if electron-conducting (n-type or acceptor) conjugated polymers can be developed with suitable absorption bands, electronic structures, and high electron mobilities, they could contribute to light harvesting in polymer/polymer (all-polymer) blend BHJ solar cells.[14−31] In such all-polymer solar cells, the efficiency of hole transfer from the photoexcited acceptor polymer to the donor polymer could be as important to the charge photogeneration process as is the photoinduced electron transfer from the donor to acceptor polymer.[32−34] Understanding of the detailed photophysics and mechanisms of charge photogeneration in polymer/polymer blend solar cells has not yet advanced to the same level as in polymer/fullerene devices in part because of the limited availability of high-mobility n-type semiconducting polymers.

Early studies of all-polymer solar cells were limited to bilayer planar heterojunction devices because of limited processability of the n-type or p-type polymers.[19,35,36] Acceptor polymers based on cyano-functionalized poly(*p*-phenylenevinylene)s (CN-PPVs) allowed the study of polymer/polymer blend BHJ solar cells, demonstrating high open circuit voltages ($V_{oc}$) (~1 V), but the efficiencies were limited by low photocurrents.[19,37,38] n-Type semiconducting copolymers derived from 2,1,3-benzothiadiazole moiety have also been explored in all-polymer BHJ solar cells, giving rise to only moderate efficiencies (<2%).[39−41] More recently, availability of perylene diimide (PDI)- and naphthalene diimide (NDI)-based n-type

Received: October 2, 2014
Revised: February 26, 2015
Published: March 11, 2015





DOI: 10.1021/ma502042k
Macromolecules 2015, 48, 1759−1766

semiconducting polymers has enabled the demonstration of polymer/polymer blend BHJ solar cells with improved power conversion efficiencies (~3−5%).[15−18,28,29,42] Nevertheless, new n-type semiconducting polymers, besides NDI- and PDI-based materials, are needed both to enable a broader understanding of structure−photovoltaic relationships and to facilitate improvement of performance of all-polymer solar cells.

In this paper, we report a study of all-polymer blend solar cells based on the recently introduced tetraazabenzodifluoranthene diimide (BFI)[43] derivative n-type conjugated polymer semiconductor[44] as the electron acceptor component of the active blend layer. The two-dimensional (2D) $\pi$-conjugated BFI polymers, exemplified by the 2,5-thienylene-linked PBFI-T (Chart 1), were shown to exhibit unipolar n-type charge transport with field-effect electron mobility as high as 0.3 $cm^2/(V\ s)$.[44] However, their electron-accepting and photovoltaic properties in all-polymer solar cells are yet to be reported. Encouraged by the recent finding that selenophene-linked naphthalene diimide (NDI) copolymers had a superior performance in photovoltaic devices compared to the corresponding thiophene-linked NDI copolymer (Figure S1),[15,28,29] we herein also report the synthesis and evaluation of a new selenophene-linked BFI copolymer, PBFI-S (Chart 1), as an acceptor in all-polymer blend solar cells. A known p-type semiconducting polymer, poly[(4,4′-bis(2-ethylhexyl)dithieno-[3,2-*b*:2′,3′-*d*]silole)-2,6-diyl-*alt*-(2,5-bis(3-(2-ethylhexyl)-thiophen-2-yl)thiazole[5,4-*d*]thiazole)] (PSEHTT, Chart 1),[45,46] was used as the electron donor paired with PBFI-T or PBFI-S in the all-polymer blend solar cells. We found that PBFI-T:PSEHTT blend solar cells had a power conversion efficiency (PCE) of 2.60%, whereas the corresponding PBFI-S:PSEHTT cells had a PCE of 0.75%. We show that this unexpected factor of 3.5 difference in the photovoltaic efficiencies of PBFI-T and PBFI-S devices largely originates from the reduced driving energy for hole transfer in the latter blend system, among other factors. The bulk charge transport in the blend films was investigated by the space-charge-limited current (SCLC) technique. Finally, the bulk and surface morphologies of the two photovoltaic blend systems were respectively probed by grazing incidence wide-angle X-ray scattering (GIWAXS) and atomic force microscopy (AFM) imaging.

**Chart 1. Molecular Structures of Acceptor Polymers (PBFI-T and PBFI-S) (a) and the Donor Polymer (PSEHTT) (b)**

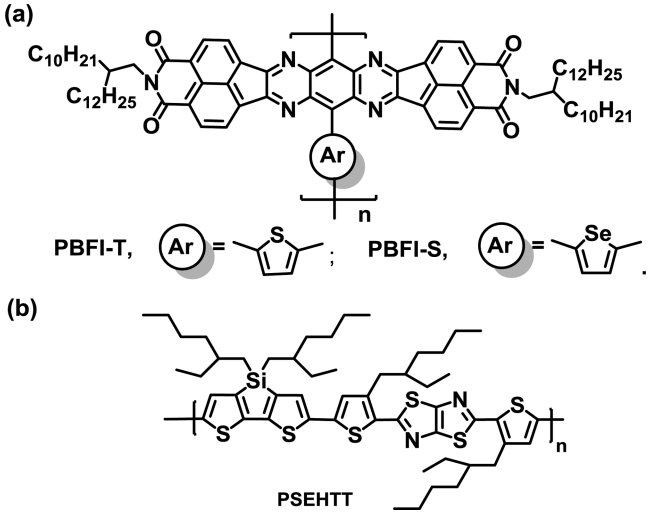


## RESULTS AND DISCUSSION

**Synthesis, Optical Absorption, and Electronic Structure.** The new n-type semiconducting polymer, PBFI-S, was synthesized via the Stille cross-coupling copolymerization of the previously reported 8,17-dibromo-7,9,16,18-tetraazabenzodifluoranthene-3,4,12,13-tetracarboxylic acid diimide (BFI-Br2) monomer[43,44] with 2,5-bis(trimethylstannyl)selenophene,[15,47] similar to the synthesis of PBFI-T.[44] PBFI-S has excellent solubility in common organic solvents (chloroform, chlorobenzene, toluene, etc.) at room temperature. The number-average molecular weight ($M_n$) of PBFI-S, as determined by gel permeation chromatography (GPC) relative to polystyrene standards, is 29.3 kDa with a polydispersity index (PDI) of 3.55. The sample of previously synthesized PBFI-T, which is investigated here alongside PBFI-S, has an $M_n$ of 61.0 kDa and a PDI of 3.16. Similar to PBFI-T,[44] PBFI-S has excellent thermal stability with an onset thermal decomposition temperature ($T_d$) of 430 °C from thermogravimetric analysis (TGA) experiments in flowing nitrogen. Differential scanning calorimetry (DSC) scans in the 20−400 °C range did not show any thermal transitions for either polymer, suggesting that melting temperatures may be higher than 400 °C.

Figure 1 shows the thin film absorption spectra of the n-type polymers PBFI-T and PBFI-S as well as that of the p-type polymer PSEHTT. The absorption profile of PBFI-S is very similar to that of PBFI-T; both have a high-energy band with identical $\lambda_{max}$ centered at 380 nm ($\alpha$ = 7.3 × $10^4$ $cm^{-1}$). However, the lower energy absorption band of PBFI-S has a $\lambda_{max}$ = 948 nm ($\alpha$ = 1.7 × $10^4$ $cm^{-1}$), which is significantly red-shifted (>100 nm) from that of PBFI-T.[44] The absorption edge optical band gap ($E_g$) of PBFI-S (1.13 eV) is much smaller than that of PBFI-T ($E_g$ = 1.38 eV). The highest occupied molecular orbital (HOMO)/lowest unoccupied molecular orbital (LUMO) energies of PBFI-T and PBFI-S were determined from the onset oxidation and reduction potentials, respectively, from cyclic voltammograms (Figure 2). The HOMO/LUMO energy levels of the proposed donor polymer PSEHTT[45] are also shown in Figure 2c for comparison. PBFI-T and PBFI-S have deep LUMO energy levels of −3.78 and −3.82 eV, and the same HOMO energy levels of −5.59 eV, potentially providing sufficient driving energy for photoinduced charge transfer and charge separation in blends with PSEHTT. Observation of different optical band gaps but similar HOMO/LUMO energy levels for PBFI-S and PBFI-T suggests that the two polymers have different reorganization energies and different exciton binding energies.

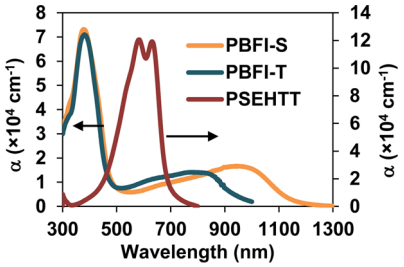


**Figure 1.** Thin film optical absorption spectra of n-type polymers (PBFI-T and PBFI-S) and p-type polymer (PSEHTT).



DOI: 10.1021/ma502042k
*Macromolecules* 2015, 48, 1759−1766

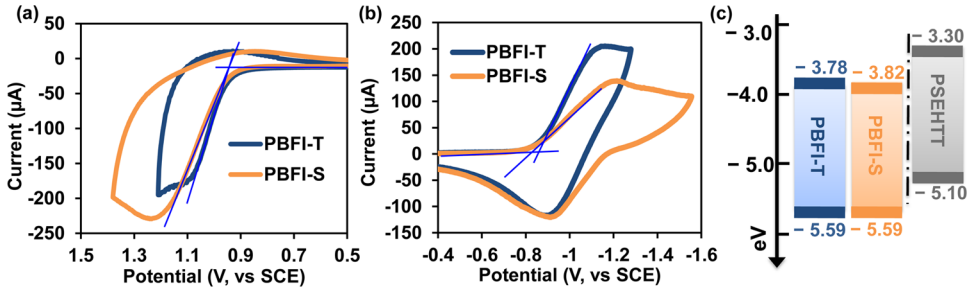


**Figure 2.** Oxidation (a) and reduction (b) cyclic voltammograms of PBFI-T and PBFI-S solid films (in 0.1 M of tetrabutylammonium hexafluorophosphate in $CH_3CN$ with $Fc^+/Fc$ as the internal reference).

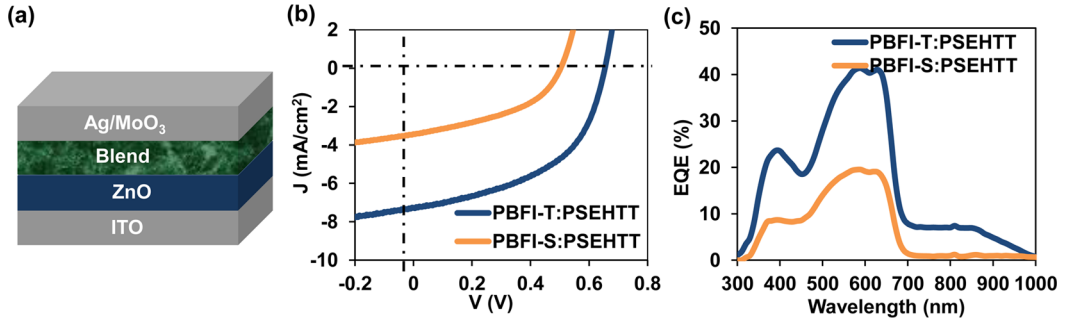


**Figure 3.** Schematic of the inverted all-polymer BHJ solar cell (a), *J*–*V* curves (b), and EQE spectra (c) of PBFI-S:PSEHTT and PBFI-T:PSEHTT blend solar cells.

**Table 1. Summary of Photovoltaic Properties and SCLC Carrier Mobilities of PBFI-T:PSEHTT and PBFI-S:PSEHTT Blends**[a]

| blend | $J_{sc}$ (mA/cm$^2$) | $V_{oc}$ (V) | FF | PCE (%) | $\mu_e$ (cm$^2$/(V s)) | $\mu_h$ (cm$^2$/(V s)) |
|---|---|---|---|---|---|---|
| PBFI-T:PSEHTT | 7.34 (7.28 ± 0.06) | 0.67 (0.67 ± 0.00) | 0.52 (0.52 ± 0.01) | 2.60 (2.50 ± 0.10) | $2.2 \times 10^{-6}$ | $4.8 \times 10^{-5}$ |
| PBFI-S:PSEHTT | 3.43 (3.35 ± 0.08) | 0.51 (0.51 ± 0.00) | 0.43 (0.43 ± 0.01) | 0.75 (0.74 ± 0.01) | $4.6 \times 10^{-8}$ | $2.7 \times 10^{-5}$ |

[a]Active layers were deposited from the PBFI-X (X = T or S):PSEHTT (2:1 w/w) blend solutions in chlorobenzene, respectively, followed by annealing at 175 °C for 10 min.

**Photovoltaic Properties.** Inverted BHJ solar cells with the structure of indium tin oxide (ITO)/zinc oxide (ZnO)/polymer blend/molybdenum trioxide ($MoO_3$)/Ag (Figure 3a) were fabricated to evaluate the photovoltaic properties of the new acceptor polymers (PBFI-T and PBFI-S) based on the PSEHTT donor polymer. The current density (*J*)–voltage (*V*) characteristics were measured under AM 1.5G solar illumination at 1 sun (100 mW/cm$^2$) in ambient air. The active layer with a blend composition of PBFI-T:PSEHTT (2:1 w/w) showed the optimal performance with a PCE of 2.60%, short circuit current ($J_{sc}$) of 7.34 mA/cm$^2$, open circuit voltage ($V_{oc}$) of 0.67 V, and fill factor (FF) of 0.52 (Figure 3b and Table 1). In stark contrast, although the optimal PBFI-S:PSEHTT devices consisted of the same blend ratio of 2:1 (w/w), their performance was significantly lower with PCE = 0.75%, $J_{sc}$ = 3.43 mA/cm$^2$, $V_{oc}$ = 0.51 V, and FF = 0.43 (Figure 3b). This large difference in performance between PBFI-S and PBFI-T devices is due to the large disparities in $V_{oc}$, $J_{sc}$, and PCE; in the case of the PCE, PBFI-T cells are a factor of 3.5 superior to those of PBFI-S. These large differences in photovoltaic properties of otherwise two very similar n-type polymer semiconductors is very surprising and not obvious from their absorption spectra (Figure 1) and electronic structures (Figure 2c).

The external quantum efficiency (EQE) spectra of both PBFI-T:PSEHTT and PBFI-S:PSEHTT blend solar cells are shown in Figure 3c. The EQE spectrum of the PBFI-T:PSEHTT photodiode shows that the photocurrent turns on at about 950 nm and has peaks of 24% at 380–420 nm and 42% at 560–680 nm. The spectrum covers a broad range from 300 to 950 nm, suggesting that both donor (PSEHTT) and acceptor (PBFI-T) polymers contributed to the photocurrent (Figure 3c). The $J_{sc}$ calculated from the EQE spectrum is 6.94 mA/cm$^2$, which is within 6.0% in agreement with the direct *J*–*V* measurement. The EQE spectrum of PBFI-S:PSEHTT photodiode turns on at around 700 nm, close to the absorption edge of PSEHTT, suggesting that the longer wavelength absorption of PBFI-S did not contribute to photocurrent (Figure 1). The intensity of the EQE spectrum in the 300–700 nm range is also much lower for PBFI-S:PSEHTT than PBFI-T:PSEHTT cells with peaks of 10% at 380–420 nm and 21% at 560–680 nm. The $J_{sc}$ calculated from the EQE spectrum of the PBFI-S cell is 3.21 mA/cm$^2$, which is within 6.4% agreement with that measured directly from *J*–*V* curve.

Among the possible reasons that could account for the large loss in short-circuit current ($J_{sc}$) and power conversion efficiency in going from PBFI-T acceptor to PBFI-S acceptor include (i) inefficient charge photogeneration at the PBFI-S:PSEHTT interface, (ii) poor bulk charge transport and collection in the PBFI-S blend system, (iii) blend morphology, and (iv) low molecular weight of PBFI-S. A simple view of the HOMO/LUMO energy levels of both blends (Figure 2c), PBFI-T:PSEHTT and PBFI-S:PSEHTT, suggests that there is identical driving energy for charge separation via either


DOI: 10.1021/ma502042k
*Macromolecules* 2015, 48, 1759–1766

photoinduced electron transfer or photoinduced hole transfer in both blends.[32−34] However, the EQE results (Figure 3c) clearly show that there is inefficient dissociation of excitons generated in both PSEHTT and PBFI-S; in fact, light absorption in PBFI-S contributes only a small amount to the photocurrent mainly in the 350−420 nm region. Adapting the empirical expression for the free energy for photoinduced electron transfer ($\Delta G_{CT}$) in polymer/fullerene systems[32,34] to the present all-polymer systems, we have

$$\Delta G_{CT} = E_{CT} - E_g^{opt} = qV_{oc} + 0.47\ \text{eV} - E_g^{opt} \quad (1)$$

where $E_{CT}$ is the charge transfer energy, $V_{oc}$ is the value at room temperature and 1 sun illumination, $q$ is the elementary charge, and $E_g^{opt}$ is the optical band gap as determined from the optical absorption spectrum of the respective acceptor polymer (Figure 1). For the PBFI-T:PSEHTT blend system, with $E_{CT}$ of 1.12 eV and $E_g^{opt}$ of 1.38 eV we have $\Delta G_{CT} = -0.26$ eV. An $E_{CT}$ of 0.98 eV and $E_g^{opt}$ of 1.13 eV result in $\Delta G_{CT} = -0.15$ eV for the PBFI-S:PSEHTT blend system, indicating an almost 2-fold increase in free energy for charge transfer compared to the PBFI-T acceptor. We examine below the other possible contributions to the loss of photocurrent and conversion efficiency in these all-polymer solar cells by investigating bulk charge transport and morphology of the active layers.

**Bulk Charge Transport.** The bulk charge transport properties of PBFI-T:PSEHTT and PBFI-S:PSEHTT blend solar cells were investigated by using the space-charge-limited current (SCLC) measurement. Electron mobility was measured in an ITO/ZnO/active layer/LiF/Al device structure whereas hole mobility was measured in an ITO/PEDOT:PSS/active layer/Au device structure. We found that the bulk hole mobility was $4.8 \times 10^{-5}$ cm$^2$/(V s) in the PBFI-T:PSEHTT blend and $2.7 \times 10^{-5}$ cm$^2$/(V s) in the PBFI-S:PSEHTT blend (Figure 4 and Table 1), which are quite comparable for both blend systems. In contrast, a large difference was observed in the bulk electron mobility of the two blends. The electron mobility in the PBFI-T:PSEHTT blend ($2.2 \times 10^{-6}$ cm$^2$/(V s)) was nearly 2 orders of magnitude higher than that in the PBFI-S:PSEHTT blends ($4.6 \times 10^{-8}$ cm$^2$/(V s)) (Figure 4 and Table 1). The observed large difference in electron mobility between PBFI-S:PSEHTT and PBFI-T:PSEHTT is likely due to their significantly different bulk morphology as will be discussed in the Surface and Bulk Morphologies section. The relatively higher and nearly balanced bulk carrier mobilities of PBFI-T:PSEHTT blend compared to the PBFI-S:PSEHTT blend could partly explain the higher photovoltaic performance of PBFI-T:PSEHTT cells. For example, the much smaller fill factors (0.43) observed in PBFI-S:PSEHTT blends can be partly accounted for by the large difference in electron and hole mobilities in this blend. These results suggest that the poorer bulk electron transport in the active layer blend of PBFI-S:PSEHTT solar cells could partly account for the significant loss in photocurrent and power conversion efficiency compared to the corresponding PBFI-T:PSEHTT devices.

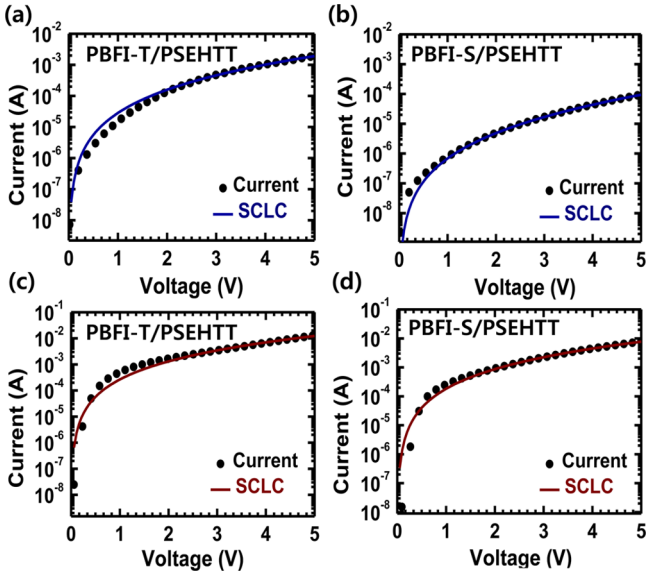


**Figure 4.** Current ($J$)−voltage ($V$) characteristics and space charge limited current (SCLC) fittings of devices measured in ambient conditions: electron-only SCLC devices of ITO/ZnO/blend/LiF/Al (a, b) and hole-only SCLC devices of ITO/PEDOT:PSS/blend/Au (c, d).

**Surface and Bulk Morphologies.** The surface and bulk morphologies of the all-polymer blend solar cells were investigated by atomic force microscopy (AFM) imaging, transmission electron microscopy (TEM), and grazing incidence wide-angle X-ray scattering (GIWAXS). AFM topographic and phase images taken directly from the surfaces of the active layers are shown in Figure 5. Both PBFI-T:PSEHTT and PBFI-S:PSEHTT blends formed good quality active layer films with smooth surfaces ($R_g$ < 1 nm) as shown in the height images (Figure 5a,c). The phase images in Figure 5b,d revealed surface features of interconnected nanoscale networks. The observed phase domains in PBFI-T:PSEHTT blend are finer than those of PBFI-S:PSEHTT blend, suggesting a greater interface area between the donor and the acceptor phases. Although the surface morphology of a polymer/polymer blend film is not necessarily identical to its bulk morphology because of the potential for vertical phase segregation,[48] the observed nanoscale phase separation and a bicontinuous network structure in the AFM images suggest that

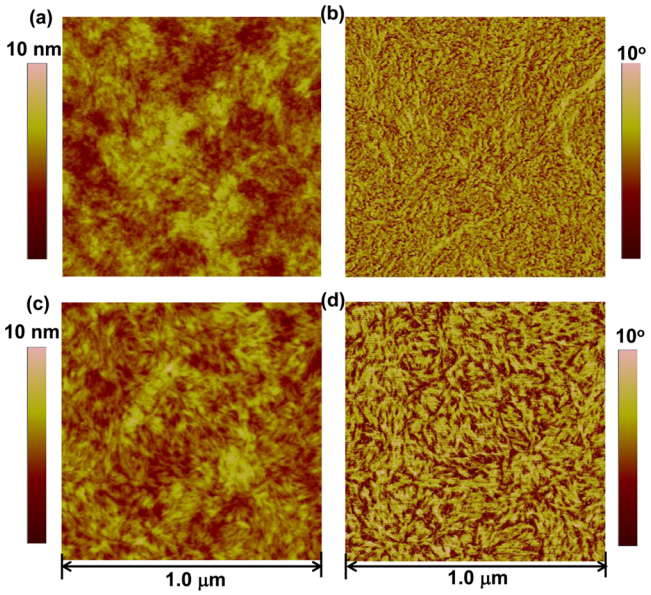


**Figure 5.** AFM topographic (a, c) and phase (b, d) images of the surface of PBFI-T:PSEHTT (a, b) and PBFI-S:PSEHTT (c, d) blend active layers.


DOI: 10.1021/ma502042k
Macromolecules 2015, 48, 1759−1766

efficient charge separation could be obtained in both all-polymer blend devices. Similar to the AFM images, a significant difference was not observed between the bright-field transmission electron microscopy (TEM) images of PBFI-T:PSEHTT and PBFI-S:PSEHTT blends (Figure S4). In other words, the observed similar surface and bulk solid morphology could not explain the observed large difference in photovoltaic properties.

To further address the electronic differences between PBFI-T and PBFI-S, we performed GIWAXS to study bulk film morphology and crystallinity. Fortunately, in blends of different polymers, each component has unique diffraction peaks that can be used to examine each polymer in the blend. Moreover, this technique yields 2D-scattering information that can be used to examine chain orientation by separately integrating the in-plane and out-of-plane components of the diffraction patterns (Figure S5). For this study, the pure PBFI-T and PBFI-S polymers show diffraction patterns typical of semicrystalline conjugated polymers[49,50] with lamellar (100) and $\pi-\pi$ stacking (010) peaks at 0.22 and 1.5 Å$^{-1}$, respectively (Figure 6). There

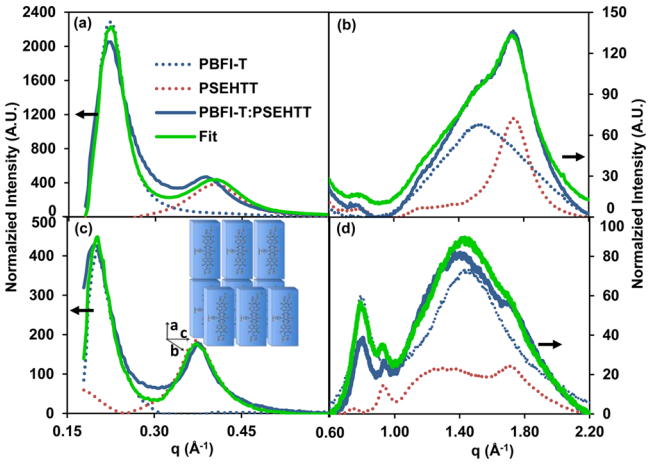


**Figure 6.** GIWAXS radially averaged scattering patterns for PBFI-T, PSEHTT, and the PBFI-T:PSEHTT blend as well as the linear regression of the blend: (a, b) out-of-plane scattering; (c, d) in-plane scattering (inset cartoon shows the orientation of polymer chains with respect to the substrate).

is also a monomer-to-monomer repeat distance (001) peak at 0.8 Å$^{-1}$. The PBFI-T (100) peak has a higher integrated intensity out-of-plane compared to in-plane, implying an edge-on stacking motif (Figure 6a,c). The same general trend is observed for PBFI-S, but the difference in peak areas between out-of-plane and in-plane diffraction is less and the PBFI-S peaks are all broader, indicating smaller crystalline coherence lengths and less edge-on orientation in PBFI-S (Figure 7) compared to PBFI-T (Figure 6b,d). Interestingly, the (100) peaks for both PBFI-T and PBFI-S show a larger repeat distance in-plane than out-of-plane. For PBFI-T, the in-plane repeat distance is 2.9 Å larger than the out-of-plane value, and for PBFI-S, the difference is 4.1 Å. Because the out-of-plane diffraction is susceptible to artifacts caused by the specular reflection, we integrated 10° slices to determine if the shifts present between the in- and out-of-plane diffraction exists at all angles (Figure S6). Typically, the diffraction is obtained by integrating one 10° slice in both the horizontal ($xy$, in-plane) and vertical ($z$, out-of-plane) directions; here we analyzed all of the slices that span from the in-plane slice to the out-of-plane

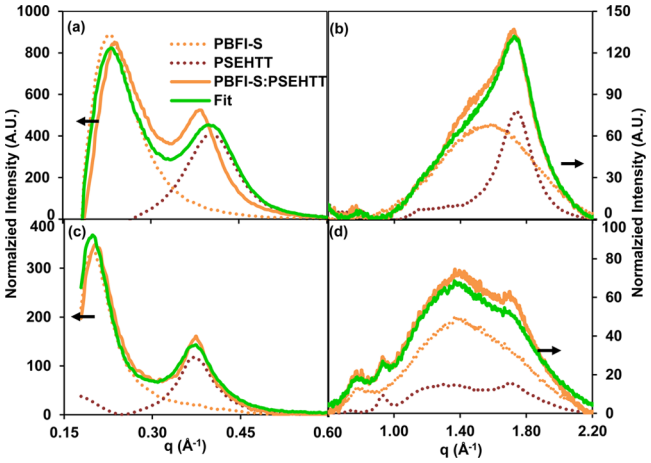


**Figure 7.** GIWAXS radially averaged scattering patterns of PBFI-S, PSEHTT, and the PBFI-S:PSEHTT blend as well as the linear regression of the blend: (a, b) out-of-plane scattering; (c, d) in-plane scattering.

slice (9 slices, 0–90°). PBFI-T and PBFI-S both show shifts in (100) and (010) peaks toward higher $q$ when integrating from in-plane to out-of-plane. The in-plane (100) and out-of-plane (010) peaks together describe polymer chains with a face-on orientation in these films. We find that the in-plane (100) is shifted to lower $q$ and the out-of-plane (010) is shifted to a higher $q$. This supports the picture where interactions with the substrate straightens polymer chains and promotes close $\pi$-stacking distances while ordering the alkyl chains on this large monomer unit, thereby causing the lamellar stacking distance to increase. By contrast, polymers with an edge-on stacking motif are described by the out-of-plane (100) peak and the in-plane (010) peak. When this large monomer unit assembles edge-on, the alkyl chains are no longer aligned, resulting in a decrease of the lamellar stacking distance and an increase in the $\pi$-stacking distance. Similar effects are observed in the PBFI-S:PSEHTT and PBFI-T:PSEHTT BHJs, where the PBFI polymer peaks and the (100) of PSEHTT shifts but the rest of the PSEHTT peaks ultimately remain unaffected. These findings indicate that the interactions with the substrate can have a significant effect on the lamellar stacking in these polymers with large monomer units, and thus shifts between the in-plane and out-of-plane diffraction are observed.

The PSEHTT shows similar diffraction, but with the lamellar diffraction peak shifted to higher $q$ because of the smaller size of the monomer unit in PSEHTT (Figure 6). For PSEHTT, peaks are observed at 0.38 Å$^{-1}$ for the (100) diffraction peak and at 1.3 and 1.7 Å$^{-1}$ for the (010) diffraction peaks (Figure 6). The two peaks likely correspond to highly ordered lamellar stacking and more disordered $\pi$-stacking domains. Again, we observe the (001) distance peak at 0.8 Å$^{-1}$. For PSEHTT, the highly ordered $\pi$-stacking peak shows distinctively greater out-of-plane scattering intensity, suggesting a face-on orientation of these domains. The less ordered $\pi-\pi$ stacking peaks show slightly higher in-plane intensity, suggesting that these domains are either edge-on or isotropic. Potentially, interactions between the polymer and the substrate help planarize polymer chains near the substrate interface, producing a smaller $\pi-\pi$ stacking distance and a distinct face-on orientation. In the bulk of the film, $\pi-\pi$ stacking distances would then be greater and the domain orientation more isotropic. Other than the changes in intensity for the two (010) peaks, no additional peak shifts are


DOI: 10.1021/ma502042k
*Macromolecules* 2015, 48, 1759–1766

observed between in-plane and out-of-plane diffractions for PSEHTT, in contrast to the results presented above for the neat PBFI-T and PBFI-S.

To a first approximation, diffraction from PBFI-T:PSEHTT (Figure 6) and PBFI-S:PSEHTT (Figure 7) blend films appear to be a linear combination of the pure polymers. The first conclusion from the diffraction data is that both PBFI-T:PSEHTT and PBFI-S:PSEHTT films are dominantly separated into mostly pure component domains. To gain more insight, the blend data were fit as a linear combination of the two pure polymers for both in-plane and out-of-plane diffraction. Figures 6 and 7 show the pure polymers, the polymer blends, and the best fit sum for both PBFI-T:PSEHTT and PBFI-S:PSEHTT blends, respectively. By comparing the out-of-plane integrated data of the polymer blend films against the linear regression fit of PBFI-T:PSEHTT, we observe a peak shift of 0.7 Å in the PSEHTT peak in Figure 6a. This indicates some mixing of PBFI-T into the pure PSEHTT domains which results in an increase in the lamellar stacking distance of PSEHTT. In contrast, the out-of-plane PBFI-T (100) peak does not shift, implying no mixing of the PSEHTT molecules into the pure PBFI-T domains. Interestingly, the in-plane data show minimal shifts for both PBFI-T and PSEHTT data when compared to the linear regression fit, as shown in Figure 6b, indicating less mixing for PSEHTT domains oriented face-on with respect to the substrate. There are no shifts in the $\pi-\pi$ stacking peaks for either PBFI-T or PSEHTT in any orientation, and the data are well fit by a linear combination of the pure polymers, indicating that polymer mixing does not disrupt the $\pi-\pi$ interactions. We note that the combined data were fit simply by scaling and adding the pure polymer patterns, and a single scaling parameter produced good agreement with the experimental data across both low- and high-$q$ regions, giving us confidence in this method.

In contrast to the PBFI-T blends, Figure 7a shows that for blends of PBFI-S with PSEHTT the out-of-plane (100) peak for PSEHTT shifts to a larger lamellar spacing by 0.7 Å and PBFI-S shifts to a smaller lamellar spacing by 0.8 Å, indicating mixing of the two polymers. For mixtures of two polymers, the lamellar spacing is generally an average of the two, with the lamellar spacing for the larger spacing polymer shifting to higher $q$ and the lamellar spacing for the smaller polymer shifting to lower $q$. This happens because a polymer with a shorter lamellar spacing allows for disordering of the polymer side chains in the polymer with the longer lamellar spacing and a decrease in the average lamellar spacing.[51,52] Overall, these shifts indicate that for edge-on domains PBFI-S can mix into PSEHTT domains and PSEHTT molecules can mix into PBFI-S domains. The in-plane diffraction for PBFI-S:PSEHTT blend film shows minimal shifts in Figure 7c,d compared to the shifts observed in the out-of-plane direction, again suggesting that face-on domains show less mixing than edge-on domains. In addition, the $\pi-\pi$ stacking peaks again appear to be a linear combination of PSEHTT and PBFI-S and do not shift.

The higher crystallinity of PBFI-T and the presence of relatively pure acceptor (PBFI-T) domains largely accounts for the higher electron mobility in the PBFI-T:PSEHTT blend, while relatively poorer crystallinity of PBFI-S and mixing of PSEHTT into the acceptor (PBFI-S) domains explain the lower electron mobility in PBFI-S:PSEHTT blends. Comparing these GIWAXS findings to device performance suggests that the presence of relatively pure PBFI-T domains is important to device performance because the PBFI-T blends show significantly higher efficiency than the PBFI-S blends. Some mixing of acceptor polymer molecules into the PSEHTT domains occurs in both systems, and it is possible that device performance could be further improved if this mixing could be reduced.

## CONCLUSIONS

The tetraazabenzodifluoranthene diimide-based n-type semiconducting polymers, PBFI-T and PBFI-S, have been investigated as new electron acceptors in polymer/polymer (all-polymer) blend solar cells. All-polymer blend solar cells using the thiophene-linked acceptor polymer (PBFI-T) with PSEHTT donor had a PCE of 2.60% with a $J_{sc}$ of 7.34 mA/cm$^2$, $V_{oc}$ of 0.67 V, and 52% FF. Although the selenophene-linked acceptor polymer (PBFI-S) has a much smaller optical band gap (1.13 eV) than the thiophene-linked acceptor polymer (PBFI-T), PBFI-S:PSEHTT blend solar cells had a much reduced performance (0.75% PCE, $V_{oc}$ = 0.61 V, and FF = 43%), showing that light harvesting by PBFI-S did not contribute significantly to photocurrent generation. Among the factors that explain the large reduction in photovoltaic efficiency of PBFI-S:PSEHTT blends compared to PBFI-T:PSEHTT blends are the reduced driving energy for charge separation ($\Delta G_{CT}$) and reduced electron mobility in the former blend system and the differences in miscibility of the polymers in the two blend systems as observed in GIWAXS experiments.

## EXPERIMENTAL SECTION

**Materials.** Tris(*o*-tolyl)phosphine and bis(dibenzylideneacetone)-palladium(0) ($Pd(dba)_2$) were purchased from Aldrich. 8,17-Dibromobenzodifluoranthene-3,4,12,13-tetracaboxylic acid diimide (BFI-$Br_2$),[43] 2,5-bistrimethylstannylselenophene,[15] and poly-[(7,9,16,18-tetraazabenzodifluoranthene-3,4,12,13-tetracarboxylic acid diimide)-8,17-diyl-*alt*-thiophene-2,5-diyl] (PBFI-T)[44] were synthesized by following the reported procedures. The synthesis of poly[(4,4′-bis(2-ethylhexyl)dithieno[3,2-*b*:2′,3′-*d*]silole)-2,6-diyl-*alt*-(2,5-bis(3-(2-ethylhexyl)thiophen-2yl)thiazolo[5,4-*d*]thiazole)] (PSEHTT)[45] was previously reported.

**Synthesis of PBFI-S.** BFI-$Br_2$ (200 mg, 0.14 mmol) and 2,5-bis(trimethylstannyl)selenophene (65 mg, 0.14 mmol) were dissolved in 20 mL of anhydrous toluene and purged with Ar for 10 min. A solution of $Pd(dba)_2$ (6 mg) and tris(*o*-tolyl)phosphine (12 mg) was added to the monomer solution. The mixture was slowly heated to reflux and kept stirring for 5 days. At the end of the polymerization, 2-tributylstannylthiophene (0.1 mL) with a solution of $Pd(dba)_2$ (3 mg) and P(*o*-tol)$_3$ (6 mg) and bromobenzene (0.15 mL) were successively added to the mixture to remove the remaining end (functional) groups. Each ending-capping reaction took 12 h. After cooling back to room temperature, the volatile materials were evaporated, and the solids were redissolved in 6 mL of toluene and precipitated into a mixture of 100 mL of methanol and concentrated HCl (20:1, v/*v*). The green solid was collected and further purified by successive Soxhlet extraction with methanol, acetone, and hexanes. Yield (126 mg, 64.4%). GPC (at 60 °C in chlorobenzene against polystyrene standards): $M_w$ = 104 kDa, $M_n$ = 29.2 kDa, PDI ($M_w/M_n$) = 3.55. $^1$H NMR ($CDCl_3$, 25 °C, 500 MHz): $\delta$ = 10.5−7.4 (br, 10H, aromatic-H), 4.6−3.7 (br, 4H, $CH_2$), 2.4−0 ppm (m, 94H). UV/vis/NIR: $\lambda_{max}$ (in $CHCl_3$, 5.2 $\mu$M) 894 nm ($\varepsilon = 3.1 \times 10^3$ M$^{-1}$ cm$^{-1}$), 378 nm ($2.0 \times 10^4$ M$^{-1}$ cm$^{-1}$); $\lambda_{max}$ (thin film) 948 nm ($1.7 \times 10^4$ cm$^{-1}$), 377 nm ($7.3 \times 10^4$ cm$^{-1}$). CV (thin film, in 0.1 M of $Bu_4NPF_6$ in $CH_3CN$): $E_{1/2}$(red) −1.06 V (irreversible), $E_{peak}$(ox) 1.23 V (irreversible). TGA ($N_2$, 10 °C/min): $T_d$ = 428 °C (onset), 55.7% residue at 800 °C. Elemental analysis calcd for $C_{86}H_{108}N_6O_4Se$: C 75.46%, H 7.95%, N 6.14%. Found: C 74.79%, H 7.84%, N 5.99%.

**Characterizations.** Gel permeation chromatography (GPC) analysis was performed using Polymer Lab Model 120 gel permeation


DOI: 10.1021/ma502042k
*Macromolecules* 2015, 48, 1759−1766

chromatograph (DRI/high sensitivity refractive index detector and PL-BV400HT viscometer) against polystyrene standards in chlorobenzene at 60 °C. Thermogravimetric analysis (TGA) of the polymers was conducted on a TA Instruments model Q50TGA at a heating rate of 10 °C/min under a flow of $N_2$ with scans from room temperature to 800 °C. Differential scanning calorimetry (DSC) analysis was performed on a TA Instruments Q100 under $N_2$ by scanning from 20 to 400 °C at a heating rate of 20 °C/min. Cyclic voltammetry was performed on an EG&G Princeton Applied Research potentiostat/galvanostat (model 273A). The CV data were analyzed by using a Model 270 Electrochemical Analysis System Software on a PC computer. A three-electrode cell was used, using platinum wire electrodes as both counter and working electrodes. A thin film of the polymer sample was drop-casted onto the working electrode from a solution of polymer in chloroform (10 mg/mL) and dried under vacuum. Silver/silver ion (Ag in 0.1 M $AgNO_3$ solution, Bioanalytical System, Inc.) was used as a reference electrode. Ferrocene was used as an internal standard with ferrocene/ferrocenium ($Fc/Fc^+$) couple at 0.16 V vs SCE. All solutions were purged with argon for 20 min before each experiment. Optical absorption spectra were collected on a PerkinElmer model Lambda 900 UV/vis/near-IR spectrophotometer.

**Fabrication and Characterization of Inverted Solar Cells.** Solutions of 20 mg/mL PSEHTT and 20 mg/mL PBFI-T in chlorobenzene were prepared separately. Then a PSEHTT:PBFI-T blend solution was prepared by mixing the two polymer solutions at a volume ratio of 1:2, followed by adding chlorobenzene to obtain a total concentration of 15 mg/mL. The PSEHTT:PBFI-S blend solution was similarly prepared. Solar cells with the inverted device structure of ITO/ZnO/active layer/$MoO_3$/Ag were fabricated. ITO substrates (10 Ω/□, Shanghai B. Tree Tech. Consult Co., Ltd., Shanghai, China) were cleaned sequentially with acetone, deionized water, and isopropyl alcohol in an ultrasonic bath and blown with nitrogen until dried, followed by oxygen plasma treatment. Zinc oxide (ZnO) precursor was prepared as reported in the literature,[53] spin-coated on top of the ITO, and annealed at 250 °C for 1 h in air. The ZnO film thickness was approximately 30 nm. The active layer was then spin-coated from the PSEHTT:PBFI-X (X = T or S) blend solution to make a thin film of ∼60−80 nm thickness and thermally annealed at 175 °C for 10 min in a glovebox. The substrates were then loaded into a thermal evaporator (BOC Edwards, 306) to deposit an anode composed of thin layer of 7.5 nm $MoO_3$ and 100 nm Ag under high vacuum ($8 \times 10^{-7}$ Torr). Five solar cells, each with an active area of 4 $mm^2$, were fabricated per ITO substrate. The current density−voltage ($J$−$V$) curves of solar cells were measured using a HP4155A semiconductor parameter analyzer under laboratory ambient air conditions. An AM 1.5G illumination at 100 $mW/cm^2$ was provided by a filtered Xe lamp and calibrated by using an NREL-calibrated Si photodiode. The external quantum efficiency (EQE) was measured by using a QEX10 solar cell quantum efficiency measurement system (PV Measurements, Inc.) and was calibrated with an NREL-certified Si photodiode before measurement.

**Space Charge Limited Current (SCLC) Measurement.** Current−voltage ($J$−$V$) characteristics of the SCLC devices were measured by using a HP4155A semiconductor parameter analyzer (Yokogawa Hewlett-Packard, Tokyo). The carrier mobility was extracted by fitting the $J$−$V$ curves in the near quadratic region according to the modified Mott−Gurney equation[54]

$$J = \frac{9}{8}\varepsilon\varepsilon_0\mu\frac{V^2}{L^3}\exp\left(0.89\beta\frac{\sqrt{V}}{\sqrt{L}}\right)$$

where $J$ is the current density, $\varepsilon_0$ is the permittivity of free space, $\varepsilon$ is the relative permittivity, $\mu$ is the zero-field mobility, $V$ is the applied voltage, $L$ is the thickness of active layer, and $\beta$ is the field activation factor.

**Grazing Incidence Wide-Angle X-ray Scattering (GIWAXS).** 2D grazing incidence wide-angle X-ray diffraction (GIWAXS) experiments were performed at the Stanford Synchrotron Radiation Lightsource (SSRL) on beamline 11-3 using a wavelength of 0.9742 Å. The beamspot was approximately 150 μm wide, and a helium chamber was utilized to reduce signal-to-noise. Samples were prepared by spinning films onto silicon substrates. The data were analyzed using the WxDiff software package.

## ■ ASSOCIATED CONTENT

### Ⓢ Supporting Information

Molecular structures of PNDIT and PNDIS, TGA trace of PBFI-S, and optical absorption of PBFI-S in chloroform. This material is available free of charge via the Internet at http://pubs.acs.org.

## ■ AUTHOR INFORMATION


### Corresponding Author

*E-mail: jenekhe@u.washington.edu (S.A.J.).


### Notes

The authors declare no competing financial interest.

## ■ ACKNOWLEDGMENTS


Synthesis of n-type conjugated polymers was supported by the NSF (DMR-1035196 and DMR-1409687). The photovoltaic studies were supported by the U.S. Department of Energy, Office of Basic Energy Sciences, Division of Material Sciences, under Award DEFG02-07ER46467. Use of the Stanford Synchrotron Radiation Lightsource, SLAC National Accelerator Laboratory, is supported by the U.S. Department of Energy, Office of Science, Office of Basic Energy Sciences, under Contract DE-AC02-76SF00515. Structural Studies were supported by the National Science Foundation Under Grant CHE-1112569. We thank Jordan Aguirre for preparation of samples for the X-ray scattering studies and Selvam Subramaniyan for providing the donor polymer PSEHTT.


## ■ REFERENCES


(1) Günes, S.; Neugebauer, H.; Sariciftci, N. S. *Chem. Rev.* **2007**, *107*, 1324−1338.
(2) Cheng, Y.-J.; Yang, S.-H.; Hsu, C.-S. *Chem. Rev.* **2009**, *109*, 5868−5923.
(3) Li, Y. *Acc. Chem. Res.* **2012**, *45*, 723−733.
(4) Liang, Y.; Xu, Z.; Xia, J.; Tsai, S.-T.; Wu, Y.; Li, G.; Ray, C.; Yu, L. *Adv. Mater.* **2010**, *22*, E135−E138.
(5) He, Z.; Zhong, C.; Su, S.; Xu, M.; Wu, H.; Cao, Y. *Nat. Photonics* **2012**, *6*, 591−595.
(6) Guo, X.; Zhou, N.; Lou, S. J.; Smith, J.; Tice, D. B.; Hennek, J. W.; Ortiz, R. P.; Navarrete, J. T. L.; Li, S.; Strzalka, J.; Chen, L. X.; Chang, R. P. H.; Facchetti, A.; Marks, T. J. *Nat. Photonics* **2013**, *7*, 825−833.
(7) Small, C. E.; Chen, S.; Subbiah, J.; Amb, C. M.; Tsang, S.-W.; Lai, T.-H.; Reynolds, J. R.; So, F. *Nat. Photonics* **2012**, *6*, 115−120.
(8) You, J.; Dou, L.; Yoshimura, K.; Kato, T.; Ohya, K.; Moriarty, T.; Emery, K.; Chen, C.-C.; Gao, J.; Li, G.; Yang, Y. *Nat. Commun.* **2013**, *4*, 1446.
(9) Li, G.; Zhu, R.; Yang, Y. *Nat. Photonics* **2012**, *6*, 153−161.
(10) Aguirre, J. C.; Ferreira, A.; Ding, H.; Jenekhe, S. A.; Kopidakis, N.; Asta, M.; Pilon, L.; Rubin, Y.; Tolbert, S. H.; Schwartz, B. J.; Dunn, B.; Ozolins, V. *J. Phys. Chem. C* **2014**, *118*, 19505−19523.
(11) Lu, L.; Xu, T.; Chen, W.; Landry, E. S.; Yu, L. *Nat. Photonics* **2014**, *8*, 716−722.
(12) Hendriks, K. H.; Li, W.; Wienk, M. M.; Janssen, R. A. J. *J. Am. Chem. Soc.* **2014**, *136*, 12130−12136.
(13) Armin, A.; Hambsch, M.; Wolfer, P.; Jin, H.; Li, J.; Shi, Z.; Burn, P. L.; Meredith, P. *Adv. Energy Mater.* **2014**, 1401221.
(14) Zhou, E.; Cong, J.; Wei, Q.; Tajima, K.; Yang, C.; Hashimoto, K. *Angew. Chem., Int. Ed.* **2011**, *50*, 2799−2803.
(15) Earmme, T.; Hwang, Y.-J.; Murari, N. M.; Subramaniyan, S.; Jenekhe, S. A. *J. Am. Chem. Soc.* **2013**, *135*, 14960−14963.




DOI: 10.1021/ma502042k
*Macromolecules* 2015, 48, 1759−1766

(16) Zhou, N.; Lin, H.; Lou, S. J.; Yu, X.; Guo, P.; Manley, E. F.; Loser, S.; Hartnett, P.; Huang, H.; Wasielewski, M. R.; Chen, L. X.; Chang, R. P. H.; Facchetti, A.; Marks, T. J. *Adv. Energy Mater.* **2014**, *4*, 1300785.
(17) Cheng, P.; Ye, L.; Zhao, X.; Hou, J.; Li, Y.; Zhan, X. *Energy Environ. Sci.* **2014**, *7*, 1351−1356.
(18) Zhou, E.; Cong, J.; Hashimoto, K.; Tajima, K. *Adv. Mater.* **2013**, *25*, 6991−6996.
(19) Kietzke, T.; Hörhold, H.-H.; Neher, D. *Chem. Mater.* **2005**, *17*, 6532−6537.
(20) Zhan, X.; Tan, Z. A.; Domercq, B.; An, Z.; Zhang, X.; Barlow, S.; Li, Y.; Zhu, D.; Kippelen, B.; Marder, S. R. *J. Am. Chem. Soc.* **2007**, *129*, 7246−7247.
(21) Holcombe, T. W.; Woo, C. H.; Kavulak, D. F. J.; Thompson, B. C.; Fréchet, J. M. J. *J. Am. Chem. Soc.* **2009**, *131*, 14160−14161.
(22) Friedel, B.; McNeill, C. R.; Greenham, N. C. *Chem. Mater.* **2010**, *22*, 3389−3398.
(23) Zhou, E.; Tajima, K.; Yang, C.; Hashimoto, K. *J. Mater. Chem.* **2010**, *20*, 2362−2368.
(24) Hwang, Y.-J.; Ren, G.; Murari, N. M.; Jenekhe, S. A. *Macromolecules* **2012**, *45*, 9056−9062.
(25) Zhou, E.; Cong, J.; Zhao, M.; Zhang, L.; Hashimoto, K.; Tajima, K. *Chem. Commun.* **2012**, *48*, 5283−5285.
(26) Yao, K.; Intemann, J. J.; Yip, H.-L.; Liang, P.-W.; Chang, C.-Y.; Zang, Y.; Li, Z. A.; Chen, Y.; Jen, A. K. Y. *J. Mater. Chem. C* **2014**, *2*, 416−420.
(27) Mori, D.; Benten, H.; Okada, I.; Ohkita, H.; Ito, S. *Adv. Energy Mater.* **2014**, *4*, 1301006.
(28) Earmme, T.; Hwang, Y.-J.; Subramaniyan, S.; Jenekhe, S. A. *Adv. Mater.* **2014**, *26*, 6080−6085.
(29) Hwang, Y.-J.; Earmme, T.; Subramaniyan, S.; Jenekhe, S. A. *Chem. Commun.* **2014**, *50*, 10801−10804.
(30) Zhou, Y.; Kurosawa, T.; Ma, W.; Guo, Y.; Fang, L.; Vandewal, K.; Diao, Y.; Wang, C.; Yan, Q.; Reinspach, J.; Mei, J.; Appleton, A. L.; Koleilat, G. I.; Gao, Y.; Mannsfeld, S. C. B.; Salleo, A.; Ade, H.; Zhao, D.; Bao, Z. *Adv. Mater.* **2014**, *26*, 3767−3772.
(31) Kozycz, L. M.; Gao, D.; Tilley, A. J.; Seferos, D. S. *J. Polym. Sci., Part A: Polym. Chem.* **2014**, *52*, 3337−3345.
(32) Ren, G.; Schlenker, C. W.; Ahmed, E.; Subramaniyan, S.; Olthof, S.; Kahn, A.; Ginger, D. S.; Jenekhe, S. A. *Adv. Funct. Mater.* **2013**, *23*, 1238−1249.
(33) Clarke, T. M.; Durrant, J. R. *Chem. Rev.* **2010**, *110*, 6736−6767.
(34) Di Nuzzo, D.; Wetzelaer, G.-J. A. H.; Bouwer, R. K. M.; Gevaerts, V. S.; Meskers, S. C. J.; Hummelen, J. C.; Blom, P. W. M.; Janssen, R. A. J. *Adv. Energy Mater.* **2013**, *3*, 85−94.
(35) Alam, M. M.; Jenekhe, S. A. *Chem. Mater.* **2004**, *16*, 4647−4656.
(36) Jenekhe, S. A.; Yi, S. *Appl. Phys. Lett.* **2000**, *77*, 2635−2637.
(37) Halls, J. J. M.; Walsh, C. A.; Greenham, N. C.; Marseglia, E. A.; Friend, R. H.; Moratti, S. C.; Holmes, A. B. *Nature* **1995**, *376*, 498−500.
(38) Yu, G.; Heeger, A. J. *J. Appl. Phys.* **1995**, *78*, 4510−4515.
(39) Mori, D.; Benten, H.; Kosaka, J.; Ohkita, H.; Ito, S.; Miyake, K. *ACS Appl. Mater. Interfaces* **2011**, *3*, 2924−2927.
(40) He, X.; Gao, F.; Tu, G.; Hasko, D.; Hüttner, S.; Steiner, U.; Greenham, N. C.; Friend, R. H.; Huck, W. T. S. *Nano Lett.* **2010**, *10*, 1302−1307.
(41) McNeill, C. R.; Abrusci, A.; Hwang, I.; Ruderer, M. A.; Müller-Buschbaum, P.; Greenham, N. C. *Adv. Funct. Mater.* **2009**, *19*, 3103−3111.
(42) Zhou, Y.; Kurosawa, T.; Ma, W.; Guo, Y.; Fang, L.; Vandewal, K.; Diao, Y.; Wang, C.; Yan, Q.; Reinspach, J.; Mei, J.; Appleton, A. L.; Koleilat, G. I.; Gao, Y.; Mannsfeld, S. C. B.; Salleo, A.; Ade, H.; Zhao, D.; Bao, Z. *Adv. Mater.* **2014**, *26*, 3767−3772.
(43) Li, H.; Kim, F. S.; Ren, G.; Hollenbeck, E. C.; Subramaniyan, S.; Jenekhe, S. A. *Angew. Chem., Int. Ed.* **2013**, *52*, 5513−5517.
(44) Li, H.; Kim, F. S.; Ren, G.; Jenekhe, S. A. *J. Am. Chem. Soc.* **2013**, *135*, 14920−14923.
(45) Subramaniyan, S.; Xin, H.; Kim, F. S.; Shoaee, S.; Durrant, J. R.; Jenekhe, S. A. *Adv. Energy Mater.* **2011**, *1*, 854−860.
(46) Xin, H.; Subramaniyan, S.; Kwon, T.-W.; Shoaee, S.; Durrant, J. R.; Jenekhe, S. A. *Chem. Mater.* **2012**, *24*, 1995−2001.
(47) Hollinger, J.; Jahnke, A. A.; Coombs, N.; Seferos, D. S. *J. Am. Chem. Soc.* **2010**, *132*, 8546−8547.
(48) Murari, N. M.; Crane, M. J.; Earmme, T.; Hwang, Y.-J.; Jenekhe, S. A. *Appl. Phys. Lett.* **2014**, *104*, 223906.
(49) Chen, D.; Nakahara, A.; Wei, D.; Nordlund, D.; Russell, T. P. *Nano Lett.* **2010**, *11*, 561−567.
(50) Chen, H.; Peet, J.; Hu, S.; Azoulay, J.; Bazan, G.; Dadmun, M. *Adv. Funct. Mater.* **2014**, *24*, 140−150.
(51) Tang, Y.; McNeill, C. R. *J. Polym. Sci., Part B: Polym. Phys.* **2013**, *51*, 403−409.
(52) Han, H.; Lee, H.; Nam, S.; Jeong, J.; Lee, I.; Kim, H.; Ha, C.-S.; Kim, Y. *Polym. Chem.* **2013**, *4*, 2053−2061.
(53) Sun, Y.; Seo, J. H.; Takacs, C. J.; Seifter, J.; Heeger, A. J. *Adv. Mater.* **2011**, *23*, 1679−1683.
(54) Murgatroyd, P. N. *J. Phys. D: Appl. Phys.* **1970**, *3*, 1488−1490.


DOI: 10.1021/ma502042k
*Macromolecules* 2015, 48, 1759−1766